

# Nanoscale

Accepted Manuscript



This is an *Accepted Manuscript*, which has been through the Royal Society of Chemistry peer review process and has been accepted for publication.

*Accepted Manuscripts* are published online shortly after acceptance, before technical editing, formatting and proof reading. Using this free service, authors can make their results available to the community, in citable form, before we publish the edited article. We will replace this *Accepted Manuscript* with the edited and formatted *Advance Article* as soon as it is available.

You can find more information about *Accepted Manuscripts* in the [Information for Authors](#).

Please note that technical editing may introduce minor changes to the text and/or graphics, which may alter content. The journal's standard [Terms & Conditions](#) and the [Ethical guidelines](#) still apply. In no event shall the Royal Society of Chemistry be held responsible for any errors or omissions in this *Accepted Manuscript* or any consequences arising from the use of any information it contains.

Cite this: DOI: 10.1039/c0xx00000x

www.rsc.org/xxxxxx

ARTICLE TYPE

## In-situ preparation of N-TiO<sub>2</sub>/graphene nanocomposite and its enhanced photocatalytic hydrogen production by H<sub>2</sub>S splitting under solar light

Ashwini P. Bhirud,<sup>a</sup> Shivaram D. Sathaye,<sup>b</sup> Rupali P. Waichal,<sup>c</sup> Jalindar D. Ambekar<sup>a</sup>, Chan -J. Park<sup>c\*</sup> and  
5 Bharat B. Kale<sup>a,\*</sup>

Received (in XXX, XXX) Xth XXXXXXXXX 20XX, Accepted Xth XXXXXXXXX 20XX

DOI: 10.1039/b000000x

Highly monodispersed nitrogen doped TiO<sub>2</sub> nanoparticles were successfully deposited on graphene (N-TiO<sub>2</sub>/Gr) by facile in-situ wet  
10 chemical method for the first time. N-TiO<sub>2</sub>/Gr has been further used for the photocatalytic hydrogen production using naturally occurring abundant source of energy i.e. solar light. The N-TiO<sub>2</sub>/Gr nanocomposite composition was optimized by varying the concentrations of dopant nitrogen and graphene (using various concentration of graphene) for utmost hydrogen production. The structural, optical and morphological aspects of nanocomposites were studied using XRD, UV-DRS, Raman, XPS, FESEM, and TEM. The structural study of nanocomposite shows existence of anatase N-TiO<sub>2</sub>. Further, the details of the components present in the composition were confirmed  
15 with Raman and XPS. The morphological study shows very tiny, 7-10 nm sized N-TiO<sub>2</sub> nanoparticles are deposited on graphene sheet. The optical study reveals drastic change in absorption edge (3.19-2.41 eV) and consequent total absorption due to nitrogen doping and presence of graphene. Considering the extended absorption edge to visible region, further these nanocomposites were used as a photocatalyst to transform hazardous H<sub>2</sub>S waste into eco-friendly hydrogen using solar light. The N-TiO<sub>2</sub>/Gr nanocomposite with 2% graphene exhibits enhanced photocatalytic stable hydrogen production i.e. ~5941 μmole h<sup>-1</sup> under solar light irradiation using just 0.2 gm  
20 nanocomposite, which is much higher as compared to P25, undoped TiO<sub>2</sub> and TiO<sub>2</sub>/Gr nanocomposite. The enhancement in the photocatalytic activity is attributed to 'N' doping as well as high specific surface area and charge carrier ability of graphene. The recycling of the photocatalyst shows the good stability of the nanocomposites. This work may provide new insights to design other semiconductor deposited graphene novel nanocomposite as a visible light active photocatalyst.

### 25 1 Introduction

With the global depletion of fossil-based energy resources, naturally occurring abundant source i.e. solar light has been considered to be a promising route to generate alternative source of energy for production of hydrogen.<sup>1,2</sup> Thus, the  
30 hydrogen is produced via H<sub>2</sub>O or H<sub>2</sub>S splitting using various semiconductor photocatalysts. It would be important to point out that H<sub>2</sub> generation can also be achieved by H<sub>2</sub>O splitting; either by photocatalysis or by electrolytic process. In the electrolytic process, some electrical energy inputs are necessary to generate  
35 H<sub>2</sub>. As against this, H<sub>2</sub>S splitting utilizes solar energy which otherwise is not being used creatively as proposed in the present work. Therefore, saving of energy and offering alternative energy

40 source makes H<sub>2</sub>S splitting to generate H<sub>2</sub> has significance and as a preferred topic of research at present. Toxic H<sub>2</sub>S gas is available abundantly as a waste from coal and petroleum industries, natural gas, oil wells and geothermal plants.<sup>3</sup> H<sub>2</sub>S can be effectively decomposed by photocatalytic process under solar  
45 light irradiation to produce hydrogen, a clean fuel. Therefore, H<sub>2</sub>S splitting will not only effectively harness the abundant solar energy but also clean up the environment.

It is quite understood that solar light driven photocatalysis by semiconductor has immense importance in the  
50 area of water purification and catalysis. Among various semiconductor photocatalysts such as TiO<sub>2</sub>, ZnO, CdS, MoS<sub>2</sub>,<sup>4</sup> titania has attracted much attention due to its fascinating

properties namely, biological and chemical inertness, cost-effectiveness, and long-term stability against photocorrosion and chemical corrosions.<sup>5</sup> The band gap of TiO<sub>2</sub> is 3.2 eV and hence not effective for visible light driven photocatalysis. Therefore, using pure TiO<sub>2</sub>, the solar energy conversion would be unreasonable. Additionally, fast recombination rate of the photo-induced electron-hole pairs in pure TiO<sub>2</sub> reduces the efficiency of the photocatalytic reactions significantly, thus limiting its practical applications. Hence, many researchers tried to dope TiO<sub>2</sub> with transition metals and investigated photocatalytic activity.<sup>6</sup> However, it is found that such doping created a number of defect-states which act as the recombination centers of photogenerated electrons and holes which becomes detrimental for the photocatalysis process. Therefore, creating suitable defect states that would be favorable in three different ways, namely, 1) enhancing visible light absorption 2) improving charge separation and 3) improving overall photocatalytic reaction by facilitating charge carrier-substrate interaction which is a challenging problem. Considering the drawbacks of metal doping, anionic doping in TiO<sub>2</sub> has received much attention. The anionic doping is expected to tune the band gap of TiO<sub>2</sub> well within the visible region of solar spectrum, which enhances the absorption in visible light and consequently producing maximum number of charge carriers. Additionally, it is reported that 'p' orbitals of these dopants significantly overlap with the valence band O2p orbitals in TiO<sub>2</sub> which suppress the recombination of charge carriers (electron-holes) and enhancing the photocatalytic activity.<sup>7</sup> Nevertheless, still the progress in enhancing quantum yield and suppression of recombination of photogenerated electron-hole pairs is not satisfactory.<sup>8</sup> Another common method for enhancing the photocatalytic efficiency of TiO<sub>2</sub> is by preventing the agglomeration of catalyst nanoparticles. A method of achieving this is by confining the particle growth process in the pores or at the interface of co-adsorbents such as mesoporous materials, zeolites, alumina, silica or carbon-based or carbonaceous materials.<sup>9</sup> Such immobilization increases the surface area available for the catalytic process. Among these, carbonaceous materials are of great interest due to their unique pore structure, electronic properties, absorption capacity and charge carrier mobility. These materials include carbon nanotubes, activated carbon and graphene.<sup>10-12</sup>

As it is well known that graphene is an attractive and significant material due to its two-dimensional nanostructure with

remarkable properties specifically, superior mechanical strength, excellent mobility of charge carriers, high thermal conductivity and large specific surface area.<sup>13-16</sup> These outstanding features attracted graphene to be utilized as a promising support material to disperse and stabilize N-TiO<sub>2</sub> nanoparticles which in turn enhance the photocatalytic hydrogen production by water splitting.<sup>17</sup> One of the most critical parameters that affect the photocatalytic properties of N-TiO<sub>2</sub>/Gr composite is the interfacial contact between the graphene sheet and N-TiO<sub>2</sub> nanoparticles. Although, there are many reports on TiO<sub>2</sub>/Gr composite as photocatalyst<sup>18</sup> many of these associated to dye degradation using UV/Vis light. H<sub>2</sub> generation using UV/Vis light by photocatalysis or electro-catalysis through water/H<sub>2</sub>S splitting need more specific parameters as compared to dye degradation. Therefore the comparison of these works would be superfluous. The present study reports the use of TiO<sub>2</sub>/Gr composite as a solar light photocatalyst for H<sub>2</sub> production through H<sub>2</sub>S splitting.

To the best of our knowledge, there are few reports on N-TiO<sub>2</sub>/Gr composites used for photocatalytic and other applications. Shengang Xu and Shaokui Cao<sup>17</sup> synthesized nanocomposites of graphene oxide with nitrogen doped TiO<sub>2</sub> via hydrothermal method for photocatalytic hydrogen production by water splitting. N. R. Khalid and Zhanglian Hong<sup>19</sup> prepared nitrogen doped TiO<sub>2</sub> nanoparticles decorated on graphene sheets by low temperature hydrothermal method for methyl orange dye degradation. Jingquan Liu, Dongjiang Yang and Ziyang Huo<sup>20</sup> prepared nitrogen doped TiO<sub>2</sub>/Gr nanohybrids for dye-sensitized solar cell (DSSC). Considering the very limited study on N-TiO<sub>2</sub>/Gr composites synthesis and its applications for hydrogen production in general and by H<sub>2</sub>S splitting in particular, we have attempted an in-situ preparation of N-TiO<sub>2</sub> graphene nanocomposite and its photocatalytic application for hydrogen production under solar light.

In the present investigation, in-situ preparation of deposition of highly mono-dispersed tiny nanoparticles of N-TiO<sub>2</sub> on multi-layer of graphene sheets using facile wet chemical method has been demonstrated which is hitherto unattempted. The structural and optical properties of these nanostructures have been studied thoroughly. The prepared N-TiO<sub>2</sub>/Gr nanocomposites showed wider spectral response and higher photocatalytic activity in the visible-light region than P25, undoped TiO<sub>2</sub> and TiO<sub>2</sub>/Gr composite. We are reporting for the

first time the enhanced photocatalytic activity of N-TiO<sub>2</sub>/Gr composites for photodecomposition of H<sub>2</sub>S under solar light illumination for hydrogen generation.

## 2 Experimental part

### Preparation of Graphene oxide (GO)

Graphene oxide was prepared from graphite powder (99.99% S d fine) by a Hummers and Offeman method.<sup>21</sup>

### Preparation of Nitrogen doped TiO<sub>2</sub>/graphene (N-TiO<sub>2</sub>/Gr)

N-TiO<sub>2</sub>/Gr was prepared by using a simple wet chemical method. Analytical grade Titanium tetrachloride (TiCl<sub>4</sub>), urea and absolute ethanol were purchased from the local chemical manufacturer (Qualigene chemicals) and used as received. In a typical synthesis, the as prepared GO, (0.5%, 1%, 2% and 4%) was dispersed in a absolute ethanol and ultrasonicated for half an hour [Solution A]. A solution of 0.05 mole of TiCl<sub>4</sub> and 0.2 mole urea (1:4 w/w of TiCl<sub>4</sub>:urea) was prepared in absolute ethanol with constant stirring until a homogeneous solution was achieved [solution B]. Then, solution B was slowly added into solution A with constant stirring. The stirring was continued for additional half an hour. This final solution was then kept in oven at 150°C to obtained the black product i.e Ti-urea-graphene intermediate complex, which was found to be hygroscopic. The hygroscopic product was preserved in a desiccator and then further subdivided for heat treatment at 300°C, 400°C, 500°C and 600°C for 3h to obtain the desired products, which were no longer hygroscopic. Simultaneously, undoped TiO<sub>2</sub>, N-TiO<sub>2</sub> and TiO<sub>2</sub>-Gr were prepared for comparison, following the same procedure. The undoped TiO<sub>2</sub> was synthesized by preparing a solution of 0.05 mole TiCl<sub>4</sub> in absolute ethanol (without any additives like urea) followed by heating it at 150°C to obtained the product which was further annealed at 300°C for 3h and denoted as T1. We synthesized N-TiO<sub>2</sub> samples using different TiCl<sub>4</sub>:urea ratios i.e. 1:2, 1:4 and 1:6 (w/w) were also prepared and the better results are obtained for 1:4 ratio. The N-TiO<sub>2</sub> was prepared by heat treating homogeneous 0.05 mole TiCl<sub>4</sub> and 0.2 mole urea (1:4 w/w of TiCl<sub>4</sub>:urea) solution in absolute ethanol at 150°C to obtained an intermediate product (Ti-urea complex) which was further annealed at 300°C, 400°C and 500°C for 3h. The product annealed at 300°C is named as T2. We discuss the results of the final product i.e. N-TiO<sub>2</sub>/Gr with that of T2. The TiO<sub>2</sub>/Gr sample was prepared by heat treating 0.05 mole TiCl<sub>4</sub> and as prepared

GO (with 2% loading) in absolute ethanol (without any additives, i.e. urea) at 150°C to obtained the intermediate product which was further annealed at 300°C for 3h and denoted as T3. The other products with dopants and graphene composites with 0.5%, 1% and 2% loading of GO were annealed at 300°C for 3h and denoted as T4, T5 and T6, respectively. After annealing, all the samples were washed with copious amounts of hot distilled water until all chlorine is removed and these products were then subjected to XRD, UV-DRS, Raman, XPS, FTIR, FESEM, TEM and BET, PL analysis for their characterization.

### Photodecomposition of H<sub>2</sub>S

The cylindrical quartz photochemical reactor was filled with 200 ml 0.25 M aqueous KOH and purged with argon for 1 h. Hydrogen sulphide (H<sub>2</sub>S) was bubbled through the solution for about 1 h at the rate of 2.5 ml min<sup>-1</sup> at 299 K. Undoped TiO<sub>2</sub>, N-TiO<sub>2</sub>, TiO<sub>2</sub>/Gr and N-TiO<sub>2</sub>/Gr (0.2 g) was introduced into the reactor and irradiated with a solar light source Xe-lamp (300 W, LOT ORIEL GRUPPE, EUROPA, LSH302) with constant stirring. The escaped hydrogen sulfide was trapped in a NaOH solution. The amount of hydrogen gas evolved was collected in a graduated cylinder and measured. The evolved hydrogen was then analyzed for its purity using a gas chromatograph (Model Shimadzu GC-14B, MS-5 Å column, TCD, Ar carrier). All the samples (T1–T6) were tested for their catalytic activity under identical conditions. In an experiment, a composite was tested as a catalyst for a continuous period of 420 minutes (7 hrs.).

### Characterization

The crystalline phases and the crystallite size of the photocatalyst was identified using an X-ray powder diffraction (XRD) technique (XRD-D8, Advance, Bruker-AXS) with Cu K $\alpha$  radiation. The optical properties of the powder samples were studied using an UV-visible-near infrared spectrometer (UV-VIS-NIR, Perkin Elmer Lambda-950). Room temperature micro Raman scattering (RS) was performed using a HR 800-Raman Spectroscopy, Horiba Jobin Yvon, France, with an excitation at 632.81 nm by a coherent He–Ne ion laser and a liquid nitrogen cooled CCD camera to collect and process the scattered data. The nature of chemical bonds formed in N-TiO<sub>2</sub> and reduction of GO to graphene were examined using X-ray photoelectron spectroscopy (XPS, ESCA-3000, VG Scientific Ltd, England) with a base pressure greater than  $1.0 \times 10^{-9}$  Pa and Mg K $\alpha$

radiation (1253.6 eV) was used as an X-ray source operated at 150 W. FTIR spectra's were recorded with a Nicolet Magna 550 spectrometer. The morphologies of the N-TiO<sub>2</sub>/Gr composites nanostructures were characterized by field emission scanning electron microscopy (FESEM, Hitachi, S-4800) and high resolution transmission electron microscopy (HRTEM, JEOL, 2010F). For HRTEM studies, samples were prepared by dispersing the powder in acetone, followed by sonication in an ultrasonic bath for 2 min and then drop-casting the dispersion on a carbon coated copper grid and by subsequent drying in a vacuum. The Brunauer-Emmett-Teller (BET) specific surface area ( $S_{\text{BET}}$ ) of the powders was analyzed by nitrogen adsorption in a Micro-meritics ASAP 2020 nitrogen adsorption apparatus (U.S.). All of the prepared samples were degassed at 180°C prior to nitrogen adsorption measurements. Photoluminescence (PL) emission spectra were recorded using HORIBAJOBINYVON, F-3 Fluorescence spectrophotometer.

### 3 Results and discussion

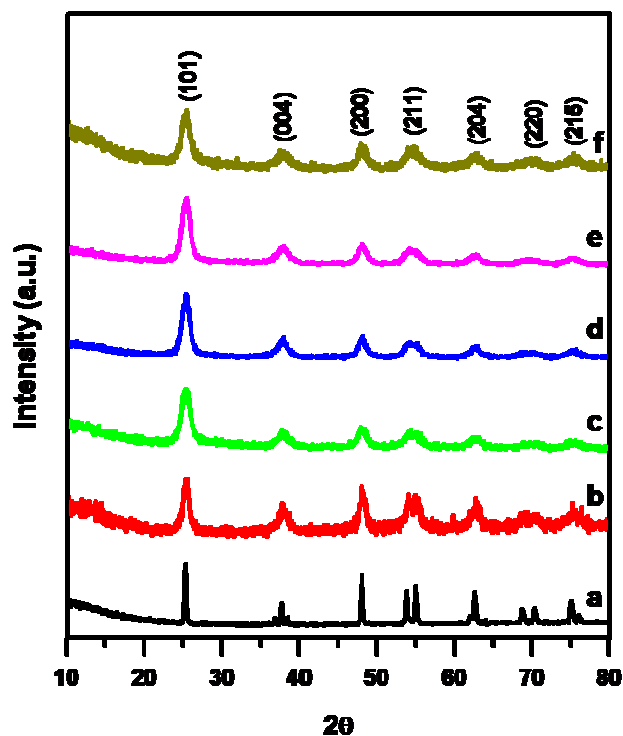
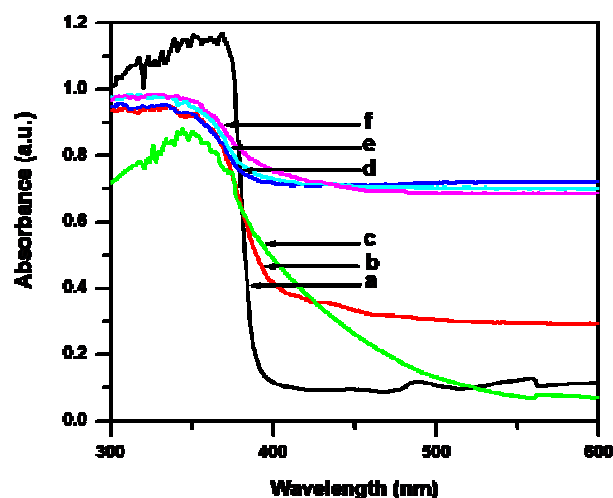


Fig. 1 XRD spectrum of samples (a) undoped TiO<sub>2</sub> (T1) treated at 300°C for 3h (b) N-TiO<sub>2</sub> treated at 300°C for 3h (T2) (c) TiO<sub>2</sub>/Gr composite with 2% loading which treated at 300°C for 3h (T3) and N-TiO<sub>2</sub>/Gr composites treated at 300°C for 3h with different GO loading (d) 0.5% (T4), (e) 1% (T5) and (f) 2% (T6)

Fig. 1 shows the XRD pattern for the N-TiO<sub>2</sub>/Gr nanocomposites (T4-T6) synthesized with different content of graphene which is compared with the N-TiO<sub>2</sub> (T2), TiO<sub>2</sub>/Gr (T3) and TiO<sub>2</sub> (T1). The peaks observed at 25.3°, 37.8°, 48.0°, 55.1°, 62.7°, 70.3° and 75.0° are indexed as (101), (004), (200), (211), (204), (220) and (215) planes respectively, clearly reveals the formation of anatase (JCPDS no. 21-1272) crystallites. No peaks were observed for carbon species (multi-layer graphene) in the composite samples T3-T6, which may be due to low amount of graphene.<sup>22</sup> Further, observation indicates that the full width at half maximum (FWHM) is more for the anatase peaks of N-TiO<sub>2</sub> (T2) which is attributed to the induction of nitrogen into the TiO<sub>2</sub> lattice. In case of samples (T3-T6), the presence of increasing amount of graphene may play an additional role in restricting the degree of crystallization.<sup>23</sup> Further, the existence of graphene and its consequential effects is supported by Raman and XPS analysis.

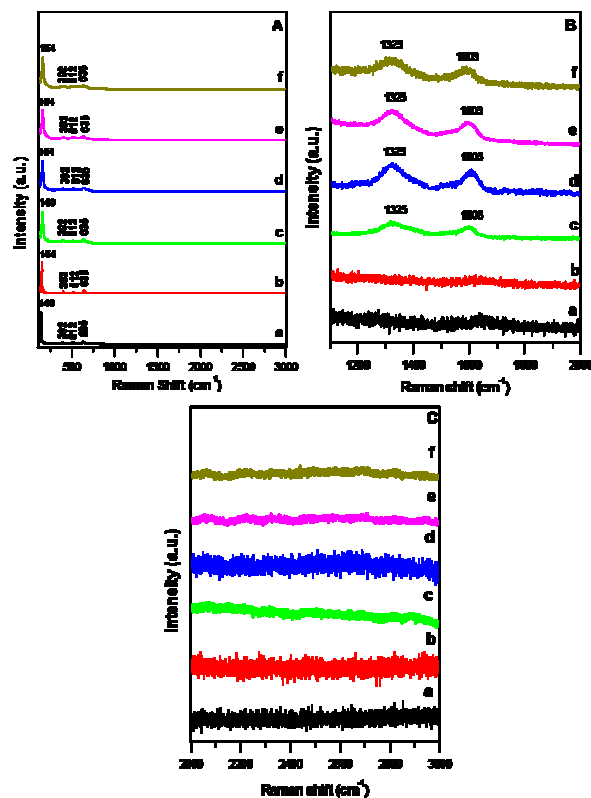
Generally, the overall photocatalytic activity of a semiconductor is mainly related to the optical absorption ability in the desired spectral region, efficient separation of photogenerated electrons, holes and fast transport of the photogenerated electrons and holes to the surface which ultimately decreases the recombination.

Fig. 2 shows the UV-Vis diffuse reflectance spectra (UV-DRS) of undoped TiO<sub>2</sub> (T1), N-TiO<sub>2</sub> (T2), TiO<sub>2</sub>/Gr (T3) and N-TiO<sub>2</sub>/Gr (T4-T6) composite catalysts. The spectra shows the absorption edge at 388 nm (3.19 eV) for undoped TiO<sub>2</sub> (T1) as commonly observed for anatase TiO<sub>2</sub>. The band gap energies of samples T2-T6 were determined to be 2.93 (423 nm), 2.60 (476 nm), 2.56 (485 nm), 2.53 (490 nm), 2.41 (515 nm) eV, respectively. The optical absorption shows a red-shift with the incorporation of 'N' dopant.<sup>24</sup> In addition, the extended visible light absorption edge was observed with increasing the graphene content in composite samples.<sup>24a</sup> It is obvious that N-TiO<sub>2</sub>/Gr shows much stronger absorption of visible light than TiO<sub>2</sub>/Gr composite. When 'N' was introduced into TiO<sub>2</sub>/Gr composite, the absorption edge of T6 sample is extended to 515 nm (2.41eV).<sup>25</sup> These observations are comparable to TiO<sub>2</sub>-CNT and C-doped TiO<sub>2</sub>.<sup>26</sup> Also, it is reported that "black" TiO<sub>2</sub> with defect structure shows absorption in visible region. Additionally, the extension of the absorption edge to the visible region may also be due to 'O' deficiencies occurred during in-situ preparation where carbon may be acting as a reducing agent at high temperatures.<sup>27</sup>



**Fig. 2** UV-DRS spectra of samples (a) undoped TiO<sub>2</sub> (T1) treated at 300°C for 3h (b) N-TiO<sub>2</sub> treated at 300°C for 3h (T2) (c) TiO<sub>2</sub>/Gr composite with 2% loading which treated at 300°C for 3h (T3) and N-TiO<sub>2</sub>/Gr composites treated at 300°C for 3h with different GO loading (d) 0.5% (T4), (e) 1% (T5) and (f) 2% (T6)

Raman spectroscopy is one of the most useful techniques for analyzing the ordered/disordered crystalline structures of carbonaceous and titanium oxide-based materials.



**Fig. 3**(A, B, C) Raman spectrum of samples (a) undoped TiO<sub>2</sub> (T1) treated at 300°C for 3h (b) N-TiO<sub>2</sub> treated at 300°C for 3h (T2) (c) TiO<sub>2</sub>/Gr composite with 2% loading which treated at 300°C for 3h (T3) and N-TiO<sub>2</sub>/Gr composites treated at 300°C for

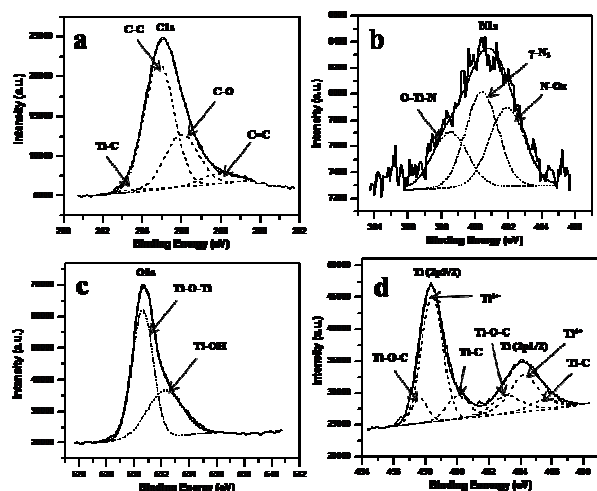
3h with different GO loading (d) 0.5% (T4), (e) 1% (T5) and (f) 2% (T6). (B) shows the magnified range from 1100-2000 cm<sup>-1</sup>. (C) shows the magnified range from 2000-3000 cm<sup>-1</sup>.

Fig. 3(A) shows a comparison of the Raman spectra of undoped TiO<sub>2</sub> (T1), N-TiO<sub>2</sub> (T2), TiO<sub>2</sub>/Gr (T3) and N-TiO<sub>2</sub>/Gr (T4-T6) samples (composites). In case of GO (Fig. S1), Raman spectrum shows two typical bands located at 1325 and 1591 cm<sup>-1</sup>, which correspond to disordered sp<sup>2</sup> carbon (D-band) and well ordered graphite carbon structures (G-band), respectively.<sup>28</sup> As for undoped TiO<sub>2</sub> (T1), several characteristic bands at 140, 392, 512, and 635 cm<sup>-1</sup> which correspond to the Eg (1), B1g(1), A1g+B1g(2) and Eg(2) modes of anatase, respectively.<sup>28b, 29</sup> For the N-TiO<sub>2</sub> (T2), TiO<sub>2</sub>/Gr (T3) and N-TiO<sub>2</sub>/Gr (T4-T6) composites, all the above mentioned Raman bands for anatase are observed. Additionally, for samples T3-T6, Raman spectrum shows the presence of D (1325 cm<sup>-1</sup>) and G (1603 cm<sup>-1</sup>) bands of graphene, indicating successful incorporation of graphene in the composites TiO<sub>2</sub>/Gr (T3) and N-TiO<sub>2</sub>/Gr (T4-T6) respectively. Fig. 3(B) shows the Raman spectrum of the undoped TiO<sub>2</sub> (T1), N-TiO<sub>2</sub> (T2), TiO<sub>2</sub>/Gr (T3) and N-TiO<sub>2</sub>/Gr (T4-T6) nanocomposites exclusively in the range of 1100-2000 cm<sup>-1</sup>. It can be clearly seen that two prominent peaks centered at about 1325 cm<sup>-1</sup> (D band) and 1603 cm<sup>-1</sup> (G band) suggesting that the structure of graphene is maintained in the composite. In addition, the G band for samples (T3-T6) is broadened and red shifted to 1603 cm<sup>-1</sup> after the reduction of graphene oxide (1591 cm<sup>-1</sup>). This can be understood by considering Ti-O-C bond formation which implies a close interaction between TiO<sub>2</sub> and graphene,<sup>30</sup> and highlighting a real integration across the interface between graphene and anatase TiO<sub>2</sub>.

Generally, 2D peak of Raman spectrum, observed at ~2700 cm<sup>-1</sup>, is a reliable test to confirm the presence of a monolayer or few layer graphene<sup>31</sup>. Therefore, we tried to find the presence of 2D peak in the expanded range of 2000-3000 cm<sup>-1</sup>. Fig. 3(C) shows the Raman spectrum of the undoped TiO<sub>2</sub> (T1), N-TiO<sub>2</sub> (T2), TiO<sub>2</sub>/Gr (T3) and N-TiO<sub>2</sub>/Gr (T4-T6) nanocomposites in the range of 2000-3000 cm<sup>-1</sup>. 2D peak is not observed in the expanded range also. It is known that with increasing number of layers of graphene, 2D peak becomes broader and less intense. Beyond 5-6 layers of graphene, 2D peak is not observed. In these cases, it is reported that increased D/G intensity ratio as compared to that of GO is an indicator of the presence of graphene.<sup>32</sup>

A further observation reveals that the samples T3 and T4-T6 composite show an increased D/G intensity ratio 1.17 and 1.1, 1.23, 1.78 respectively in comparison to that of GO (0.93) (Fig. S1). This change suggests decrease in the average size of the  $sp^2$  domains and enhancement in the number of defects during reduction of the exfoliated GO to graphene in the synthesis process.<sup>28b, 33</sup> 'N' doping in  $TiO_2$ , the Raman spectra shows a shift in the  $TiO_2$  peak to the higher wavenumbers i.e. from 140 to 154  $cm^{-1}$  for samples T2, T4-T6 indicating an increase in the surface oxygen vacancies.<sup>34</sup>

X-ray photoelectron spectroscopy (XPS) measurements were performed to further investigate the chemical changes that occurred on the surface during composite formation by monitoring the signals of N, Ti, O and C to elucidate the interaction between graphene,  $TiO_2$  and N- $TiO_2$  nanoparticles.



**Fig. 4** XPS patterns of N- $TiO_2$ /Gr composite with 2% GO loading synthesized at 300°C for 3h (T6) (a) C(1s), (b) N(1s), (c) O(1s), (d)Ti(2p).

Fig. 4 shows the high resolution XPS spectra for C (1s), N (1s), O (1s) and Ti (2P) core levels of the N- $TiO_2$ /Gr composite. The XPS spectrum of C1s from GO (Fig. S2) is deconvoluted into three peaks which are ascribed to the following functional groups:  $Sp^2$  bonded carbon (C-C, 284.8 eV), epoxy/hydroxyls (C-O, 286 eV), carbonyls (C=O, 287.8 eV).<sup>35</sup> While the first peak indicates the presence of 2D carbon structure, the latter two peaks indicate the presence of high percentage of oxygen-containing functional groups. In comparison, the XPS spectrum of C(1s) from N- $TiO_2$ /Gr (Fig. 4a) shows that the peak intensity for oxygen containing functional groups substantially lowered as compared to the intensity for oxygen containing functional groups in the spectrum of GO,

suggests that GO has been converted to graphene. Furthermore, the band located at 283.6 eV can be assigned to the presence of the Ti-C bond.<sup>36</sup> Formation of the Ti-C bond can be shown by peak deconvolution of the Ti(2p) core level, as investigated in the Fig. 4 b shows the N(1s) core level spectrum where the peak at 397.5 eV can be attributed to the anionic N in O-Ti-N linkage<sup>37</sup> while a peaks at 400.4 and 401.9 eV are ascribed to the molecularly chemisorbed  $\gamma-N_2$  and N-Ox surface species respectively.<sup>38</sup> These peaks clearly indicate that nitrogen was interstitially/substitutionally doped into  $TiO_2$  lattice.<sup>39</sup> Fig. 4 c shows O(1s) narrow scan spectrum. The peaks around 530.6 eV and 532.2 eV are attributed to the Ti-O-Ti i.e. lattice oxygen and Ti-OH adsorbed on the sample surface, respectively.<sup>40</sup> As for Ti 2p (Fig. 4d) core level photoelectron spectrum, the peaks located at 458.4 eV and 464.2 eV are assigned to Ti (2p3/2) and Ti (2p1/2), respectively.<sup>41</sup> The splitting between the two peaks is 5.8 eV, indicating predominant formation of  $Ti^{4+}$  chemical state in the N- $TiO_2$ /Gr composite. Furthermore, there are two other deconvoluted peaks at binding energies of 457.6 and 463.1 eV relating to the Ti (2p3/2) and Ti (2p1/2), respectively. These two peaks can be assigned to the presence of  $Ti^{3+}$  chemical state in addition to the  $Ti^{4+}$ .<sup>42</sup> The peak deconvolution of the Ti (2p) core level indicated two other peaks centered at 465.9 and 460.3 eV (relating to the Ti (2p1/2) and Ti(2p3/2) peaks) confirms the formation of Ti-C bond.<sup>36</sup> It should be noted that, the XPS results also suggest the presence of Ti-O-C bonds in the N- $TiO_2$ /Gr composite. Since graphene sheets are excellent electron acceptors, the Ti-C and Ti-O-C bonds can act as effective channels in electron transferring from the photoexcited N- $TiO_2$  into the graphene sheets. Based on the peak areas of the Ti(2p), C(1s) and O(1s) core levels, the Ti/C and O/C atomic ratio obtained in the N- $TiO_2$ /Gr (T6) composite was around 0.20 and 0.98, respectively which is compared with the literature.<sup>43</sup> The presence of small amount of hydrophilic groups on the surface of graphene, such as hydroxyl and carboxyl groups, can enhance the photocatalytic activity.<sup>44</sup>

The reduction of oxygen-containing groups in GO and interaction between the  $TiO_2$  and graphene during the synthesis process was also shown by FTIR spectroscopy.

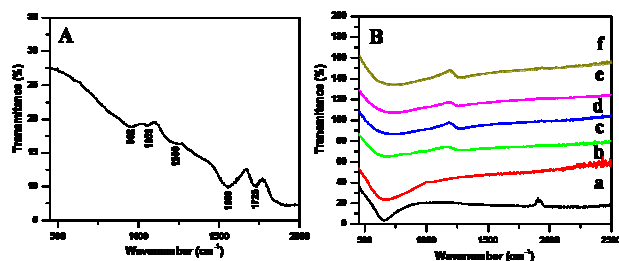
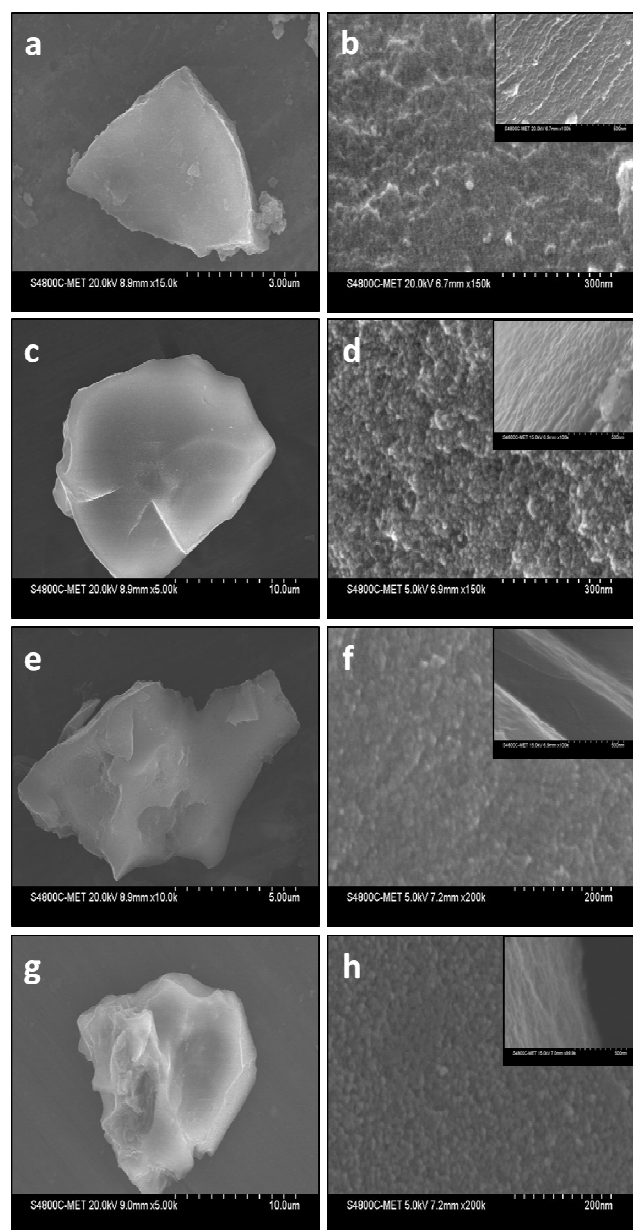


Fig. 5(A, B) FTIR spectra of samples (A) GO, (B) (a) undoped TiO<sub>2</sub> (T1) treated at 300°C for 3h (b) N-TiO<sub>2</sub> treated at 300°C for 3h (T2) (c) TiO<sub>2</sub>/Gr composite with 2% loading which treated at 300°C for 3h (T3) and N-TiO<sub>2</sub>/Gr composites treated at 300°C for 3h with different GO loading (d) 0.5% (T4), (e) 1% (T5) and (f) 2% (T6).

It could be seen that the initial GO (Fig. 5 A) displayed several characteristic absorption bands of oxygen containing groups. The IR absorption at 1725 cm<sup>-1</sup> could be attributed to the C=O stretching vibration. The peak at around 962 cm<sup>-1</sup>, 1059 cm<sup>-1</sup>, 1250 cm<sup>-1</sup> corresponds to the epoxy stretching, alkoxy C-O stretching and C-O-C stretching peaks, respectively.<sup>44, 45</sup> The broad band at 1560 cm<sup>-1</sup> can be assigned to in-plane vibrations of aromatic C=C Sp<sup>2</sup> hybridized carbons. As against the evidence of these oxygen-containing groups of GO, the absence/ negligibly small intensity of bands of oxygen containing functional groups (C-O, C-O-C) in samples (T3-T6) was noteworthy (Fig. 5B).<sup>45b</sup> Of course T1 and T2 samples show presence of sharp Ti-O-Ti bands in their IR studies at 650 cm<sup>-1</sup>. obviously, oxygen containing groups mentioned above must have reacted with the species which are in close contact with GO, namely Ti. However, the broadening of Ti-O-Ti peak suggests the presence of a peak due to Ti-O-C bond. Thus, Ti-O-Ti bonding is well understood. However, it is reported that Ti-O-C bond also forms during the low temperature synthesis at 200°C which is lower than the processing temperature in present procedure.<sup>46</sup> However, separate existence of Ti-O-C bond is not reflected in FTIR spectra which is reported to appear at 798 cm<sup>-1</sup>. Thus, broad bands due to Ti-O-Ti and Ti-O-C overlap and do not show their separate existence. The existence of Ti-O-C bonds suggests the chemical bonds were firmly built between graphene and N-TiO<sub>2</sub> nanostructures<sup>47</sup> which is supported by the XPS study.

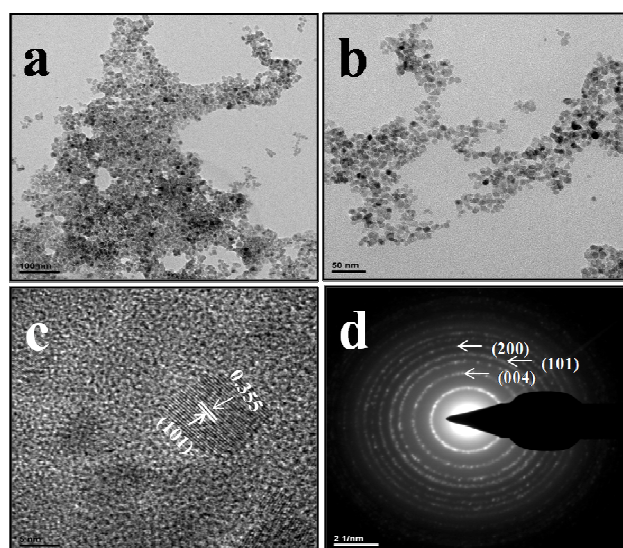
The morphology and microstructure of the GO, undoped TiO<sub>2</sub> (T1), N-TiO<sub>2</sub> (T2), TiO<sub>2</sub>/Gr (T3) and N-TiO<sub>2</sub>/Gr (T4-T6) samples were investigated by scanning electron microscopy (SEM) and transmission electron microscopy (TEM).

Fig. S3 (a, b) shows the FESEM image of GO with smooth surface. Fig S3 (c, d) shows the FESEM image of undoped TiO<sub>2</sub> (T1) with size 30-150 nm and Fig. S3 (d, e) shows the tiny nanoparticles of N-TiO<sub>2</sub> (T2). TiO<sub>2</sub>/Gr composite (T3) sample (Fig. 6 a, b) shows the TiO<sub>2</sub> nanoparticles with size ~10 nm are well dispersed on graphene sheet. The important observations are 1) pure TiO<sub>2</sub> particle size is largest among the composites, 2) during the process of doping, particle size is lowered, 3) with the inclusion of graphene in the composite, particle size is ~7-10 nm, 4) the particles on multi-layers of graphene sheets are well dispersed and remain firmly adhered to it. Fig. 6 c-h shows that the N-TiO<sub>2</sub>/Gr composite with increasing percentage of graphene (T4-T6) shows well dispersed N-TiO<sub>2</sub> nanoparticles on graphene sheet. The cross section of samples T3-T6 are shown in inset Fig. 6 (b, d, f, h) which clearly shows that ~7-10 nm N-TiO<sub>2</sub> nanoparticles confirms the same observation. The absence of any agglomeration suggests that such process is prevented by firm bonding of N-TiO<sub>2</sub> particles to graphene. This intimate interaction becomes important to facilitate photogenerated electron to get transferred from TiO<sub>2</sub> or N-TiO<sub>2</sub> nanoparticles to graphene sheets during the photo-excitation process which will be discussed later.



**Fig. 6** FESEM of samples (a,b) TiO<sub>2</sub>/Gr composite with 2% loading which treated at 300°C for 3h (T3) and N-TiO<sub>2</sub>/Gr composites treated at 300°C for 3h with different GO loadings (c,d) 0.5% (T4), (e,f) 1% (T5) and (g,h) 2% (T6).

The microstructure of N-TiO<sub>2</sub> (T2) and N-TiO<sub>2</sub>/Gr (T6) samples was further studied by TEM and HRTEM. Fig. 7 shows the TEM images of the N-TiO<sub>2</sub> (T2) and Fig. 8 shows the typical TEM images of N-TiO<sub>2</sub>/Gr (T6) sample.



**Fig. 7** TEM of N-TiO<sub>2</sub> which treated at 300°C for 3h (T2)

The TEM images (Fig. 7 a, b) we observed ~ 5-10 nm sized nanoparticles. The HRTEM image (Fig. 7c) shows clear lattice fringes of N-TiO<sub>2</sub> nanoparticles with 'd' spacing of ca. 0.355 nm which corresponds to (101) lattice plane of the anatase TiO<sub>2</sub>. The electron diffraction (Fig. 7d) shows (004), (101) and (200) planes of the anatase TiO<sub>2</sub>.

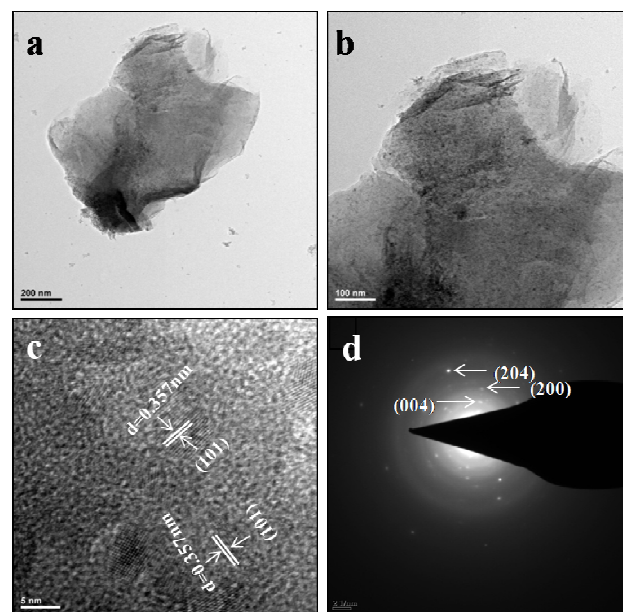


**Fig. 8** TEM of N-TiO<sub>2</sub>/Gr composite with 2% GO loading which treated at 300°C for 3h (T6)

A large number of monodispersed N-TiO<sub>2</sub> nanoparticles with an average size of 7-10 nm were observed on the graphene sheet (Fig 8 a, b). This can be attributed to the interaction between the hydrophilic functional groups (e.g. -OH, -COOH) on graphene and the hydroxyl groups on N-TiO<sub>2</sub>. The

HRTEM image (Fig. 8c) shows clear lattice fringes of individual N-TiO<sub>2</sub> particle with 'd' spacing of ca. 0.357 nm which corresponds to (101) lattice planes of the anatase TiO<sub>2</sub>. The selected area electron diffraction (SAED) pattern (Fig. 8d) indicates that the composite consists of crystalline phases. The three inside diffraction spots are assigned correspond to the (004), (200) and (204) planes of the anatase TiO<sub>2</sub>. These observations are in close agreement with the XRD results (Fig. 1).

The substantial role of graphene sheets in the formation mechanism of the N-TiO<sub>2</sub>/Gr nanocomposite is illustrated in four steps in Fig. 9.

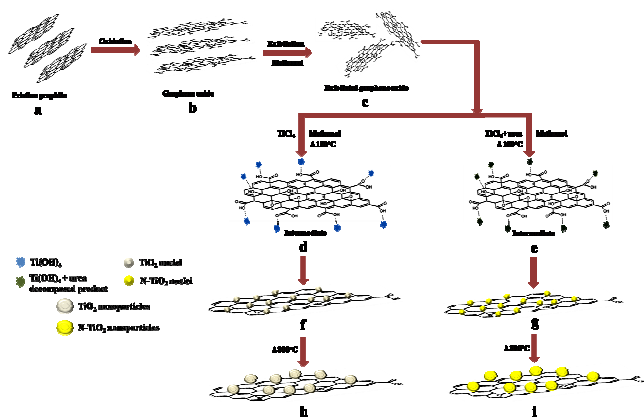


**Fig. 9** Schematic representation of formation mechanism of TiO<sub>2</sub>/Gr and N-TiO<sub>2</sub>/Gr composites

Briefly, GO is prepared using the Hummer's method via pristine graphite (Fig. 9b) and titanium tetrachloride were mixed in an absolute ethanol solvent for the formation of TiO<sub>2</sub>/Gr composite (T3). For the synthesis of N-TiO<sub>2</sub>/Gr composites (T4-T6), the GO prepared using the Hummer's method and titanium tetrachloride along with urea were mixed in an absolute ethanol solvent. During ultrasonic pretreatment, (Fig. 9c) strong van der Waals interactions among the GO layers is overcome which leads to the separation of GO sheets. Simultaneously, titanium tetrachloride and urea which are present in the same solvent interact with oxygen containing species of GO, and the resulting complex species gets anchored on oxygen site of GO possibly through hydrogen bonding or via chemisorptions.<sup>48</sup> Also, GO is reduced to graphene by ammonia released from urea at moderately high temperatures.<sup>49</sup> Further, raising the temperature, titanium tetrachloride reacts with urea and form Ti(OH)<sub>4</sub> through hydrolysis of Ti precursor by ammonia.

At the same time, urea and urea decomposed products are formed along with Ti(OH)<sub>4</sub> (Fig. 9d, e). Since, alcoholic hygroscopic urea is the reaction medium, adsorbed atmospheric

moisture facilitates the reactions mentioned above (formation of Ti(OH)<sub>4</sub>). Simultaneously, a complex consisting of Ti containing species and urea based species decompose to form TiO<sub>2</sub> on subsequent heating at temperatures >150°C. However, nitrogen species from urea is in close proximity to Ti species in the said complexes. Concomitantly, surrounding gaseous medium of ammonia also may contribute for nitrogen to be a part of TiO<sub>2</sub> lattice leading to the formation of N-TiO<sub>2</sub> nuclei (Fig. 9g). In absence of urea, obviously, only TiO<sub>2</sub> nuclei are formed (Fig. 9f). Thus, the TiO<sub>2</sub> or N-TiO<sub>2</sub> nuclei are formed on graphene and as the reaction continue to 300°C, the TiO<sub>2</sub> or N-TiO<sub>2</sub> nuclei grow which suppress agglomeration (Fig. 9h, i).

N-TiO<sub>2</sub> nanocrystals anchored on the surface of graphene sheets look like a thin film and have a larger surface area. This can offer more active adsorption sites and photocatalytic reaction centers. Therefore, it is expected to offer an enhanced photocatalytic activity.

The effect of graphene on the BET surface area of the as prepared composite samples was also investigated. As shown in Table 1, N-TiO<sub>2</sub>/Gr composite samples (T4-T6) show higher BET surface area (207.53 - 219.98 m<sup>2</sup>g<sup>-1</sup>) than undoped TiO<sub>2</sub> (T1) (109.75 m<sup>2</sup>g<sup>-1</sup>), N-TiO<sub>2</sub> (T2) (157.70 m<sup>2</sup>g<sup>-1</sup>) and TiO<sub>2</sub>/Gr (T3) (118.89 m<sup>2</sup>g<sup>-1</sup>). In the composite samples, BET surface area (S<sub>BET</sub>) increases with the increase of graphene content, which is associated with the average densities of samples.<sup>50</sup> The planar density of graphene is 0.77 mg cm<sup>-2</sup>, and the density of TiO<sub>2</sub> is 4.26 g cm<sup>-3</sup>. Therefore, the average densities of composite samples decrease with increasing graphene content, resulting in the increase of the BET surface area. However, the catalytic reaction is expected to occur on TiO<sub>2</sub> particles only. In the absence of graphene, TiO<sub>2</sub> particles would have agglomerated with a rise in density and lowered specific surface area for reaction to occur. This process is completely circumvented by graphene, making greater specific surface area. Another important feature of graphene is the recombination of separated charge carriers can be suppressed if any of the charge carriers is transported away from the photoactive material. Graphene's high electronic conductivity suits for this process leading to an enhancement of the photocatalytic performance.<sup>51</sup>

photoluminescence (PL) spectra of semiconductors are useful to investigate the migration, transfer and recombination processes of photogenerated electron-hole pairs. The PL emission

mainly originates from the recombination of the excited electrons and holes.<sup>52</sup>

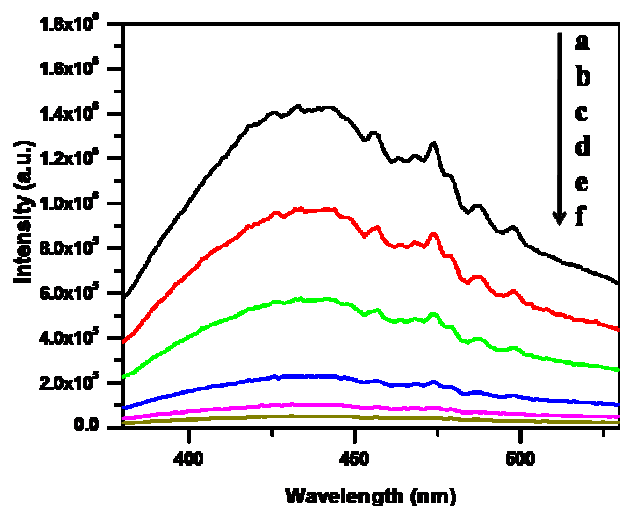


Fig. 10 PL spectra of samples (a) undoped TiO<sub>2</sub> (T1) treated at 300°C for 3h (b) N-TiO<sub>2</sub> treated at 300°C for 3h (c) TiO<sub>2</sub>/Gr composite with 2% loading which treated at 300°C for 3h (T3) and N-TiO<sub>2</sub>/Gr composites treated at 300°C for 3h with different GO loading (d) 0.5% (T4), (e) 1% (T5) and (f) 2% (T6)

Fig. 10 illustrates PL spectra of undoped TiO<sub>2</sub> (T1), N-TiO<sub>2</sub> (T2), TiO<sub>2</sub>/Gr (T3) and N-TiO<sub>2</sub>/Gr (T4-T6) monitored at an excitation wavelength of 325 nm. One peak at around 435 nm was observed for these samples, which is attributed to the recombination of holes and electrons in the valence band and conduction band. We observed that the position of peak is at 435 nm for all composites. The PL intensity of undoped TiO<sub>2</sub> (T1) is the highest among all the samples indicates the high probability of electron and hole recombination. The emission intensities were significantly weakened with N doping and graphene introduction, which implies that the recombination of charge carriers was effectively decreased, since, carriers have an alternative path, for example photocatalytic reaction. Among all the samples the lowest photoluminescence intensity was observed for T6 sample, indicating that the electron-hole recombination on the surface of catalysts is largely inhibited to generate more photoelectrons and holes to participate in the photocatalytic reactions. We therefore conclude that the enhanced photocatalytic activity of T6 sample is mainly attributed to more effective charge separation through trap formation in TiO<sub>2</sub> and transportation to graphene.

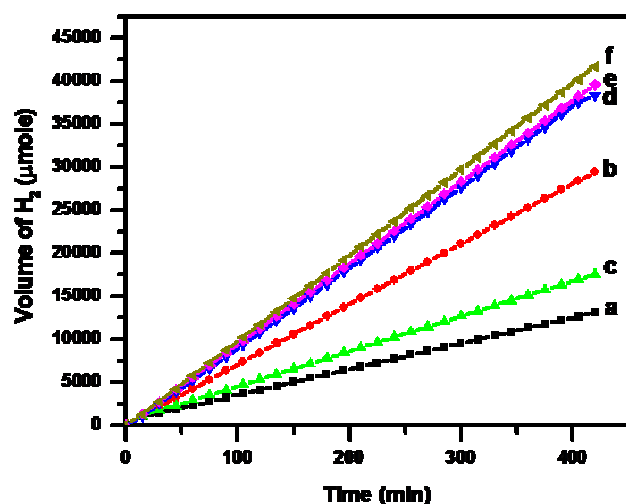
The photocatalytic activity of freshly prepared undoped TiO<sub>2</sub> (T1), N-TiO<sub>2</sub> (T2), TiO<sub>2</sub>/Gr (T3) and N-TiO<sub>2</sub>/Gr (T4-T6) samples were performed for hydrogen generation via photodecomposition of H<sub>2</sub>S using solar light.

Table 1 shows the hydrogen evolution rate from the photodecomposition of H<sub>2</sub>S using undoped TiO<sub>2</sub> (T1), N-TiO<sub>2</sub> (T2), TiO<sub>2</sub>/Gr (T3) and N-TiO<sub>2</sub>/Gr (T4-T6). Control experiments indicated that no appreciable hydrogen is produced in the absence of irradiation or photocatalyst samples, implying that hydrogen is produced only through photocatalytic reaction. Sample P25 and undoped TiO<sub>2</sub> (T1) shows hydrogen evolution rate ~1583 μmole h<sup>-1</sup> and ~1910 μmole h<sup>-1</sup> respectively, which is lower than the other samples. N-TiO<sub>2</sub>/Gr (T6) shows highest hydrogen evolution rate ~5941 μmole h<sup>-1</sup> for 420 minutes i.e. 7 hours. N-TiO<sub>2</sub> (T2) sample (without graphene) shows hydrogen evolution rate of around ~4219 μmole h<sup>-1</sup>. Thus, it can be inferred that N doping in TiO<sub>2</sub> enhances hydrogen evolution rate by ~2.2 times. Further improvement is observed by incorporating graphene in the composition i.e. sample N-TiO<sub>2</sub>/Gr (T6) which is optimized for graphene addition (Fig. S4), shows the enhanced hydrogen evolution rate which is ~3.1 times that of undoped TiO<sub>2</sub> (T1). It is also observed that the hydrogen evolution increases with increasing graphene content (see Table 1). However, further increasing the amount of graphene affects the hydrogen production which is unfavorable beyond 2%. We suggest that active sites of N-TiO<sub>2</sub> may get covered by excess graphene. Indeed, it is also reported that the excessive addition of black color graphene will lead to shielding of the active sites on the catalyst surface and also rapidly decrease the intensity of light through the depth of the reaction solution, thus resulting in the decreased photoactivity.<sup>53</sup> Because of the rapid recombination between conduction band (CB) electrons and valence band (VB) holes resulting in small number of “active” electrons/holes for the desired reaction in case of N-TiO<sub>2</sub>. Hence, lower activity obtained in case of N-TiO<sub>2</sub> without graphene is quite understood.

**Table 1:** Summary of graphene content, surface area and hydrogen evolution for 420 minutes i.e. 7 hours of synthesized samples

Sample code	Graphene content (%)	$S_{\text{BET}}$	$H_2$ ( $\mu\text{mole h}^{-1}$ )
T1	-	109.75	1910
T2	-	157.70	4219
T3	2	118.89	2543
T4	0.5	207.53	5520
T5	1	210.74	5645
T6	2	219.98	5941

undoped  $TiO_2$  (T1) treated at  $300^\circ\text{C}$  for 3h, N- $TiO_2$  treated at  $300^\circ\text{C}$  for 3h (T2),  $TiO_2/\text{Gr}$  composite treated at  $300^\circ\text{C}$  for 3h (T3) and N- $TiO_2/\text{Gr}$  composites treated at  $300^\circ\text{C}$  for 3h with different GO loading (T4), (T5), (T6)



**Fig. 11** Time versus volume of  $H_2$  ( $\mu\text{mole}$ ) evolution of samples (a) undoped  $TiO_2$  (T1) treated at  $500^\circ\text{C}$  for 3h (b) N- $TiO_2$  treated at  $300^\circ\text{C}$  for 3h (c)  $TiO_2/\text{Gr}$  composite with 2% loading which treated at  $300^\circ\text{C}$  for 3h (T3) and N- $TiO_2/\text{Gr}$  composites treated at  $300^\circ\text{C}$  for 3h with different GO loading (d) 0.5% (T4), (e) 1% (T5) and (f) 2% (T6). (The weight of the photocatalyst use for each run is 0.2gm)

As seen from Fig. 11, the nitrogen doping (T2) and the graphene content (T3) has a significant influence on the photocatalytic activity of  $TiO_2$ . Taking advantage of these conclusions, it is further shown that N- $TiO_2/\text{Gr}$  (T6) shows higher activity as compared to P25, undoped  $TiO_2$ , N- $TiO_2$ . We observed good photocatalytic performance of hydrogen generation by  $H_2S$  splitting for N- $TiO_2/\text{Gr}$  (T6) as compared to

the performance of other metal oxides<sup>54</sup> and sulfide semiconductors<sup>55</sup> is reported so far. This enhancement is attributed to two factors: (1) As compared to  $TiO_2$  (T1), N- $TiO_2$  and  $TiO_2/\text{Gr}$  (T3) samples, the larger specific surface area of N- $TiO_2/\text{Gr}$  (T6) sample offers more active adsorption sites and hence more photocatalytic reaction centers. (2) In the N- $TiO_2/\text{Gr}$  system, graphene serves as an acceptor of the electrons generated in the N- $TiO_2$  semiconductor and effectively decreases the recombination probability of the photoexcited electron-hole pairs, leaving more charge carriers for hydrogen generation.

To explain the above results, a tentative mechanism is proposed for the higher  $H_2$  production activity of the N- $TiO_2/\text{Gr}$  (T6) sample as illustrated in Fig. 12.

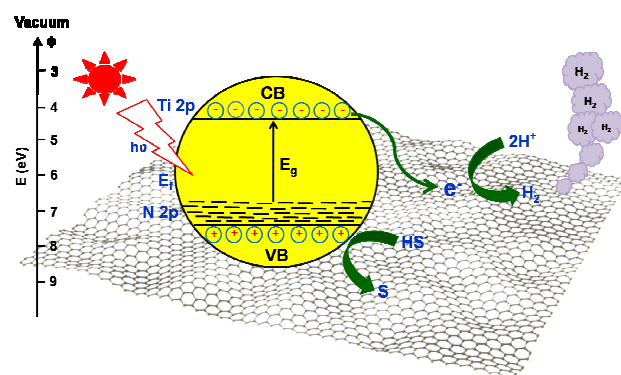
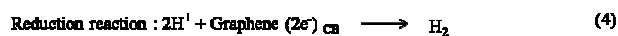
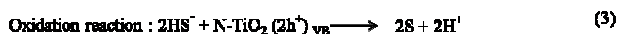
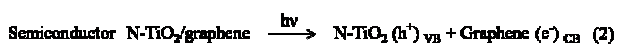


**Fig. 12** Schematic representation of photocatalytic mechanism of N- $TiO_2/\text{Gr}$  composite

In Fig. 13, N- $TiO_2$  nanoparticles are in intimate contact with graphene sheets. The intimate contact can be visualized from the synthesis procedure. During the synthesis reactions, GO gets reduced to graphene and simultaneously, there is a formation of N- $TiO_2$ . Therefore, the possibility of bond formation between  $TiO_2$  and graphene can be believed to occur. There are numerous instances in the literature wherein such bond formation has been shown to occur and has also been confirmed by FTIR and XPS study.<sup>56</sup> The nitrogen doping in  $TiO_2$  occurs when N substitutes O in the lattice. Thus, mixing of N(2p) states with O(2p) states takes place, forming a narrow impurity band near valence band of  $TiO_2$ . The optical band gap is effectively narrowed, extending the absorption in the visible region of the spectrum also.

Another important role of graphene in the composite is as an electron acceptor and transporter. Graphene has been reported to be competitive candidate as an acceptor material due to its  $\pi$ -conjugation structure and has excellent mobility of charge carriers and large specific surface area. Therefore, rapid transport

of charge carriers could be achieved and an effective charge separation consequently accomplished. Overall, both the electron accepting and transporting properties of graphene in the composite could contribute to the enhancement of photocatalytic activity.<sup>57</sup> Additionally, as per the PL study, the lower intensity peaks observed in graphene doped samples indicating that the electron-hole recombination on the surface of catalysts is largely inhibited to generate more free photoelectrons and holes. Hence, the enhanced photocatalytic activity of T6 sample is mainly attributed to more effective charge transportation and separation arisen from the strong chemical bonding of N-TiO<sub>2</sub> and graphene. The major reaction steps in this mechanism under visible-light irradiation are described in following equations.



When the as-prepared samples were irradiated by a photon of sufficient energy equal or larger than band gap, the valence electrons (e<sup>-</sup>) of anatase are excited to the CB, creating holes (h<sup>+</sup>) in the valence band VB. Normally, these charge carriers quickly recombine and only a fraction of electrons and holes participate in the photocatalytic reaction. This recombination of photo-induced electrons and holes in TiO<sub>2</sub> can be effectively lowered in the composite. The lowering of recombination effect can be explained by considering the energy level diagram of N-TiO<sub>2</sub>/graphene composite, as shown in Fig. 13. The conduction band of TiO<sub>2</sub> can be shown at -4.2 eV while valence band would be at -7.4 eV (vs. vacuum).<sup>58</sup> The work function of graphene is -4.42 eV.<sup>59</sup> Thus, transport of electrons from conduction band of TiO<sub>2</sub> to graphene is energetically a favorable process. Thus, efficiently separation of photo-induced charge carriers leads to lowering of charge recombination and effectively enhance the photocatalytic performance.<sup>60</sup> These electrons are accessible to the adsorbed H<sup>+</sup> ions (reaction 3) to form H<sub>2</sub>. Therefore, the synergistic effect of H<sub>2</sub> production on catalyst surface is because of extended visible light absorption due to 'N' doping, graphene content and efficient charge separation. To the best of our knowledge, this is the first report showing that an inexpensive carbon (graphene) material can be used as an effective co-catalyst for photocatalytic H<sub>2</sub>S splitting for H<sub>2</sub> production.

It has been reported that TiO<sub>2</sub>/graphene composite degrades on exposure to UV light and the composition changes from the original one.<sup>34</sup> On this background, as well as, usual practice in catalyst testing, it was necessary to test the catalyst for repeated reactions. Accordingly, the stability of N-TiO<sub>2</sub>/Gr composite (T6) was evaluated by performing the recycle experiments of the photocatalyst under similar conditions. After three recycles (1260 minutes i.e. 21 hours) of reaction, H<sub>2</sub> evolution did not decrease (supporting information Fig. S5). This observation indicates good stability of the catalyst for hydrogen generation for a limited period reported here. The XRD, Raman and XPS of recycled catalyst (T6) did not show any change in the phase purity and amount of graphene content, which further supports good stability of the catalyst. (Fig. S6, S7 and S8) After performing three cycles (1260 minutes i.e. 21 hours) of photocatalytic study we observed the presence of elemental 'S' and absence of 'SO<sub>4</sub>' in XPS studies (Fig. S9). The present study shows that the N-TiO<sub>2</sub> nanocomposite with graphene gives very stable photocatalytic activity and can also be used in water purification under sunlight.

## 4 Conclusion

Novel composite photocatalysts were prepared by depositing N-TiO<sub>2</sub> nanoparticles on graphene sheets by a facile in-situ wet chemical method. The well defined 7-10 nm N-TiO<sub>2</sub> nanoparticles were deposited on graphene sheet, successfully. Considering the absorption edge of N-TiO<sub>2</sub>/Gr well within visible region, the photocatalytic hydrogen production from H<sub>2</sub>S under solar light has been performed. Use of the developed catalyst demonstrated an efficient solar hydrogen production from copious, abundantly available H<sub>2</sub>S which is hitherto unattempted. The prepared N-TiO<sub>2</sub>/Gr sample showed excellent photocatalytic activity (~5941 μmoleh<sup>-1</sup>) for the hydrogen production under solar light irradiation. A suitable mechanism of the catalytic process is proposed. This study opens a new possibility in the investigation of N-TiO<sub>2</sub>/Gr composites and promotes their practical applications in environmental issues. The method investigated will also be useful for the formation of other semiconductor/graphene nanocomposite.

## Acknowledgements

The authors would like to thank Dr. D. P. Amalnerkar, Executive Director, C-MET for encouragement and nanocrystalline

materials group C-MET, Pune for their support. Ashwini P. Bhirud would like to thank Council of Scientific and Industrial Research (CSIR) for financial support. Bharat Kale and Chen Park is also thankful for the support by MSIP (ministry of science, ICT and future planning), Korea through Brain Pool Program. The authors would also like to thanks Dr. C. V. Rode and Dr K. R. Patil, NCL, Pune for BET and XPS analysis respectively. The authors are very grateful and also wish to express their gratitude to the nanocrystalline materials group C-MET, Pune for their support.

## Notes

<sup>a</sup>Centre for Materials for Electronic Technology, Panchawati, Off Pashan Road, Pune 411008, India. E-mail: \*kbbbl@yahoo.com

<sup>b</sup>759/83 Deccan Gymkhana, Pune 411004, India.

<sup>c</sup>National Chemical Laboratory (NCL), Dr. Homi Bhabha Road, Pune-411008, India.

<sup>d</sup>Department of Materials Science and Engineering, Chonnam National University 77, Yongbongro, Bukgu, Gwangju, Korea.

E-mail: \*parkej@jnu.ac.kr

†Electronic Supplementary Information (ESI) available: Raman of GO, XPS of GO, FESEM of GO, undoped TiO<sub>2</sub> and N-TiO<sub>2</sub>, graph of % graphene vs H<sub>2</sub> production, hydrogen evolution of recycled T6 sample, XRD of sample (T6) after three cycles of photocatalytic study, Raman spectrum of sample T6 after three cycles of photocatalytic study, XPS of sample (T6) after three cycles of photocatalytic study. See DOI: 10.1039/b000000x/

## References

- 1 A. Kudo, Y. Miseki, *Chem. Soc. Rev.*, 2009, **38**, 253–278.
- 2 A. Iwase, W. Y. Teoh, R. Amal, *Chem. Lett.*, 2011, **40**, 108–110.
- 3 a) M. Barbeni, E. Pelizzetti, E. Borgarello, N. Serpone, M. Gratzel and L. Balducci, *Int. J. of Hydrogen Energy*, 1985, **10**, 249–253. (b) N. Buhler, K. Meier and J. P. Reber, *J. Phy. Chem.*, 1984, **88**, 3261–3268.
- 4 H. Chang and H. Wu, *Energy Environ. Sci.*, 2013, **6**, 3483–3507.
- 5 a) Q. Li, B. D. Guo, J. G. Yu, J. R. Ran, B. H. Zhang, H. J. Yan, J. R. Gong, *J. Am. Chem. Soc.*, 2011, **133**, 10878–10884. (b) S. W. Liu, J. G. Yu, M. Jaroniec, *J. Am. Chem. Soc.*, 2010, **132**, 11914–11916. (c) Q. J. Xiang, J. G. Yu, M. Jaroniec, *Chem. Soc. Rev.*, 2012, **41**, 782–796. (d) A. L. Linsebigler, G. Q. Lu, J. T. Yates, *Chem. Rev.*, 1995, **95**, 735–758. (e) L. G. Devi, N. Kottam, S. G. Kumar, *J. Phy. Chem. C*, 2009, **113**, 15593–15601.
- 6 (a) T. Umeyashiki, T. Yamaki, H. Itoh, K. Asai, *Journal of Physics and Chem. Solids*, 2002, **63**, 1909–1920. (b) D. Dvoranova, V. Brezova, M. Mazur, M.A. Malati, *Applied Catalysis B: Environmental*, 2002, **37**, 91–105. (c) Z. Ambrus, N. Balazs, T. Alapi, G. Wittmann, P. Sipos, A. Dombi, A. mogyrosi, *Applied Catalysis B: Environmental*, 2008, **81**, 27–37.
- 7 (a) D. Tafen, J. Wang, N. Q. Wu, J. P. Lewis, *Appl. Phy. Lett.*, 2009, **94**, 09310–093103. (b) H. Irie, Y. Watanabe, K. Hashimoto, *J. Phy. Chem. B*, 2003, **107**, 5483–5486. (c) N. Serpone, *J. Phy. Chem. B*, 2006, **110**, 24287–24293. (d) J. Wang, D. N. Tafen, J. P. Lewis, Z. Hong, A. Manivannan, M. Zhi, M. Li, N. Q. Wu, *J. Am. Chem. Soc.*, 2009, **131**, 12290–12297.
- 8 (a) M. D. Hernandez-Alonso, F. Fresno, S. Suarez and J. M. Coronado, *Energy Environ. Sci.*, 2009, **2**, 1231–1257. (b) L. W. Zhang, H. B. Fu and Y. F. Zhu, *Adv. Funct. Mater.*, 2008, **18**, 2180–2189.
- 9 (a) S. Fukahori, H. Ichiura, T. Kitaoka, H. Tnaka, *Energy Environ. Sci.*, 2003, **37**, 1048–1051. (b) A. M. Turek, I. E. Wachs, E. DeCanio, *J. Phy. Chem.*, 1992, **96**, 5000–5007. (c) J. Aguado, R. Van Grieken, M.J. Lopez-Munos, J. Marugan, *J. Appl. Catal. A*, 2006, **312**, 202–212. (d) M. Li, S. Zhou, Y. Zhang, G. Chen, Z. Hong, *Appl. Surf. Sci.*, 2008, **254**, 3762–3766.
- 10 (a) G. An, W. Ma, Z. Sun, Z. Liu, B. Han, S. Miao, Z. Miao and K. Ding, *Carbon*, 2007, **45**, 1795–1801. (b) W.-J. Ong, M. M. Gui, S. -P. Chai and A. R. Mohamed, *RSC Advances*, 2013, **3**, 4505–4509.
- 11 G. Xue, H. Liu, Q. Chen, C. Hills, M. Tyrer and F. Innocent, *J. Hazard. Mater.*, 2011, **186**, 765–772.
- 12 Y. Zhang, N. Zhang, Z. R. Tang and Y. J. Xu, *Phys. Chem. Chem. Phys.*, 2012, **14**, 9167–9175.
- 13 C. Lee, X. D. Wei, J. W. Kysar, J. Hone, *Science*, 2008, **321**, 385–388.
- 14 K. I. Bolotin, K. J. Sikes, Z. Jiang, M. Klima, G. Fudenberg, J. Hone, P. Kim, H. L. Stormer, *Solid State Comm.*, 2008, **146**, 351–355.
- 15 A. A. Balandin, S. Ghosh, W. Z. Bao, I. Calizo, D. Teweldebrhan, F. Miao, C. N. Lau, *Nano Lett.*, 2008, **8**, 902–907.
- 16 M. J. McAllister, J. L. Li, D. H. Adamson, H. C. Schniepp, A. A. Abdala, J. Liu, M. Herrera-Alonso, D. L. Milius, R. Car, R. K. Prud'homme, I. A. Aksay, *Chem. Mater.*, 2007, **19**, 4396–4404.
- 17 F. Pei, Y. Liu, S. Xu, J. Lu, C. Wang, S. Cao, *Int. J. of Hydrogen Energy*, 2013, **38**, 2670–2677.
- 18 (a) G. Williams, B. Seger, P.V. Kamat, *Acs NANO*, 2008, **2**, 1487–1491. (b) H. Zhang, X. Lv, Y. Li, Y. Wang, J. Li, *Acs NANO*, 2010, **4**, 380–386. (c) Y. Zhang, Z. -R. Tang, X. Fu, Y. -J. Xu, *Acs NANO*, 2010, **4**, 7303–7314. (d) Y. Zhang, Z. -R. Tang, X. Fu, Y. -J. Xu, *Acs NANO*, 2011, **5**, 7426–7435. (e) Q. Huang, S. Tian, D. Zeng, X. Wang, W. Song, Y. Li, W. Xiao, C. Xie, *ACS Catal.*, 2013, **3**, 1477–1485. (f) Q. Xiang, J. Yu, M. Jaroniec, *Nanoscale*, 2011, **3**, 3670–3678. (g) L. Sun, Z. Zhao, Y. Zhou, L. Liu, *Nanoscale*, 2012, **4**, 613–620. (h) J. G. Radich, A. L. Krenselewski, J. Zhu, P. V. Kamat, *Chem. Mater.*, 2014, **26**, 4662–4668.
- 19 N. R. Khalid, E. Ahmed, Z. Hong, Y. Zhang, M. Ahmad, *Current Applied Physics*, 2012, **12**, 1485–1492.
- 20 R. Wang, Q. Wu, Y. Lu, H. Liu, Y. Xai, J. Liu, D. Yang, Z. Huo and X. Yao, *Appl. Mater. and Interfaces*, 2014, **6**, 2118–2124.
- 21 W. S. Hummers, R. E. Offeman, *J. Am. Chem. Soc.*, 1958, **80**, 1339.
- 22 H. Zhang, X. Lv, Y. Li, Y. Wang and J. Li, *ACS Nano*, 2010, **4**, 380–386.

- 23 S. Yoon, B. H. Ka, C. Lee, M. Park, and S. M. Oh, *Electrochem. and Solid-State Lett.*, 2009, **12**, A28-A32.
- 24 (a) Y. Zhang, Z.-R. Tang, X. Fu and Y.-J. Xu, *ACS Nano*, 2010, **4**, 7303-7314. (b) Q. Zhai, T. Bo and G. Hu, *J. Hazard. Mater.*, 2011, **198**, 78-86. (c) Z. Jiang, L. Kong, F. S. Alenazey, Y. Qian, L. France, T. Xiao and P. P. Edwards, *Nanoscale*, 2013, **5**, 5396-5402.
- 25 H. Zhang, X. Lv, Y. Li, Y. Wang, J. Li, *ACS Nano*, 2009, **4**, 380-386.
- 26 (a) N. L. Yang, J. Zhai, D. Wang, Y. S. Chen, L. Jiang, *ACS Nano*, 2010, **4**, 887-894. (b) Y. Su, Y. Xiao, Y. Li, Y. Du, Y. Zhang, *Mater. Chem. Phys.*, 2011, **126**, 761-768.
- 27 (a) N. D. Petkovich, B. E. Wilson, S. G. Rudisill, and A. Stein, *ACS Appl. Mater. Interfaces*, 2014, **6**, 18215-18227 (b) T. Yu, Y. Deng, L. Wang, R. Liu, L. Zhang, B. Tu, and D. Zhao, *Adv. Mater.*, 2007, **19**, 2301-2306 (c) C. -H. Huang, D. Gu, D. Zhao, and R. -A. Doong, *Chem. Mater.*, 2010, **22**, 1760-1767.
- 28 (a) Q. J. Xiang, J. G. Yu, M. Jaroniec, *J. Phys. Chem. C*, 2011, **115**, 7355-7363 (b) Q. J. Xiang, J. G. Yu, M. Jaroniec, *Nanoscale*, 2011, **3**, 3670-3678.
- 29 J. G. Yu, T. T. Ma, G. Liu, B. Cheng, *Dalton Trans.*, 2011, **40**, 6635-6644.
- 30 J. Yu, T. Ma and S. Liu, *Phys. Chem. Chem. Phys.*, 2011, **13**, 3491-3501.
- 31 (a) O. Akhavan, *Carbon*, 2015, **81**, 158-166 (b) I. Calizo, A. A. Balandin, W. Bao, F. Miao, C. N. Lau, *Nano Lett.*, 2007, **7**, 2645-2649.
- 32 (c) K. N. Kudin, B. Ozbas, H. C. Schniepp, R. K. Prud'homme, I. A. Aksay, R. Car, *Nano Lett.*, 2008, **8**, 36-41. (d) K. S. Kim, Y. Zhao, H. Jang, S. Y. Lee, J. M. Kim, K. S. Kim, J. -H. Ahn, P. Kim, J. -Y. Choi, B. H. Hong, *Nature*, 2009, **457**, 706-710. (e) A. C. Ferrari, J. C. Meyer, V. Scardaci, C. Casiraghi, M. Lazzeri, F. Mauri, S. Piscanec, D. Jiang, K. S. Novoselov, S. Roth, A. K. Geim, *Phys. Rev. Lett.*, 2006, **97**, 187401-187404.
- 32 (a) S. Liu, C. Liu, W. Wang, B. Cheng, J. Yu, *Nanoscale*, 2012, **4**, 3193-3200. (b) W. Wang, J. Yu, Q. Xiang, B. Cheng, *Applied Catalysis B: Environmental*, 2012, **119-120**, 109-116 (c) N. Farhangi, R. Roy Chowdhury, Y. M. Gonzalez, M. B. Ray, P. A. Charpentier, *Applied Catalysis B: Environmental* 2011, **110**, 25-32.
- 33 E. Gao, W.Z. Wang, M. Shang, J.H. Xu, *Phys. Chem. Chem. Phys.*, 2011, **13**, 2887-2893.
- 34 S. Kelly, F. H. Pollak, M. Tomkiewicz, *J. Phys. Chem. B*, 1997, **101**, 2730-2734.
- 35 O. Akhavan, M. Abdollahad, A. Esfandiari and M. Mohatashamifar, *J. Phys. Chem. C*, 2010, **114**, 12955-12959.
- 36 O. Akhavan, E. Ghaderi, *Nanoscale*, 2013, **5**, 10316-10326.
- 37 M. Satish, B. Viswanathan, R. P. Viswanath, C. S. Gopinath, *Chem. Mater.*, 2005, **17**, 6349-6353.
- 38 (a) R. Asahi, T. Morikawa, T. Ohwaki, K. Aoki, Y. Taga, *Science*, 2001, **293**, 269-271 (b) X. Wang, J. C. Tu, L. Wu, X. Fu, *Environ. Sci. Technol.*, 2006, **40**, 2369-2374.
- 39 M. Popa, D. Macovic, E. Indrea, *Microp. Mesop. Mater.*, 2010, **132**, 80-86.
- 40 N. P. Zschoerper, V. Katzenmaier, U. Vohrer, M. Haupt, C. Oehr, T. Hirth, *Carbon*, 2007, **47**, 2174-2185.
- 41 F. B. Su, X. S. Zhao, Y. Wang, J. H. Zeng, *J. Phys. Chem. B*, 2005, **109**, 20200-20206.
- 42 (a) G. An, W. Ma, Z. Sun, Z. Liu, B. Han, S. Miao, Z. Miao, K. Ding, *Carbon*, 2007, **45**, 1795-801. (b) H. Liu, W. Yang, Y. Ma, J. Yao, *Appl. Catal. A Gen.*, 2006, **299**, 218-23.
- 43 (a) O. Akhavan, E. Ghaderia, K. Rahimi, *J. Mater. Chem.*, 2012, **22**, 23260-23266. (b) Y. Zhao, D. Zhao, C. Chen, X. Wang, *J. Colloid Interf. Sci.*, 2013, **405**, 211-217.
- 44 Q. Li, B. Guo, J. Yu, J. Ran, B. Zhang, H. Yan, and J. R. Gong, *J. Am. Chem. Soc.*, 2011, **133**, 10878-10884.
- 45 (a) J. Ding, M. Wang, J. Deng, W. Gao, Z. Yang, C. Ran, X. Zhang, *Journal of Alloys and Compounds*, 2014, **582**, 29-32. (b) W. -S. Wang, D. -H. Wang, W. -G. Qu, L. -Q. Lu, A. -W. Xu, *J. Phys. Chem. C*, 2012, **116**, 19893-19901.
- 46 X. Pan, Y. Zhao, S. Liu, C. L. Korzeniewski, S. Wang, and Z. Fan, *ACS Appl. Mater. Interfaces*, 2012, **4**, 3944-3950.
- 47 (a) T. D. Nguyen-Phan, V. H. Pham, E. W. Shin, H. D. Pham, S. Kim, J. S. Chung, E. J. Kim, S. H. Hur, *Chem. Eng. J.*, 2011, **170**, 226-232. (b) A. A. Ismail, R. A. Geioushy, H. Bouzid, S. A. Al-Hajry, D. W. Bahnermann, *Appl. Catal. B: Environ.*, 2013, **129**, 62-70.
- 48 Y. B. Tang, C. S. Lee, J. Xu, Z. T. Liu, Z. H. Chen, Z. B. He, Y. L. Cao, G. D. Yuan, H. S. Song, L. M. Chen, L. B. Luo, H. M. Cheng, W. J. Zhang, I. Bello, S. T. Lee, *ACS Nano*, 2010, **4**, 3482-3488.
- 49 Z. Lei, L. Lu and X. S. Zhao, *Energy Environ. Sci.*, 2012, **5**, 6391-6399.
- 50 Q. Li, B. Guo, J. Yu, J. Ran, B. Zhang, H. -J. Yan and J. R. Gong, *J. Am. Chem. Soc.*, 2011, **133**, 10878-10884.
- 51 J. G. Yu, H. G. Yu, B. Cheng, M. H. Zhou, X. J. Zhao, *J. Mol. Catal. A*, 2006, **253**, 112-118.
- 52 J. Tang, Z. Zou, J. Ye, *J. Phys. Chem. B*, 2003, **107**, 14265-14269. (b) G. Eda, Y. -Y. Lin, C. Mattevi, H. Yamaguchi, H. -A. Chen, I. S. Chen, C.-W. Chen, M. Chhowalla, *Adv. Mater.*, 2010, **22**, 505-509.
- 53 Q. Xiang, J. Yu, *J. Phys. Chem. Lett.*, 2013, **4**, 753-759.
- 54 (a) A. P. Bhirud, S. D. Sathaye, R. P. Waichal, L. K. Nikam and B. B. Kale, *Green Chem.*, 2012, **14**, 2790-2798. (b) N. S. Chaudhari, S. S. Warule, S. A. Dhanmane, M. V. Kulkarni, M. Valant and B. B. Kale, *Nanoscale*, 2013, **5**, 9383-9390.
- 55 (a) B. B. Kale, J. O. Baeg, S. M. Lee, H. Chang, S. J. Moon and C. W. Lee, *Adv. Funct. Mater.*, 2006, **16**, 1349-1354. (b) A. P. Bhirud, N. S. Chaudhari, L. K. Nikam, R. S. Sonawane, K. R. Patil, B. J. Ook and B. B. Kale, *Int. J. Hydrogen Energy*, 2011, **36**, 11628-11639. (c) S. k. Apte, S. N. Garje, G. P. Mane, A. Vinu, A. D. Naik, D. P. Amalnerkar and B. B. Kale, *Small*, 2011, **7**, 957-964. (d) S. K. Apte, S. N. Garaje, S. D. Naik, R. P. Waichal, J. -O. Baeg, B. B. Kale, *Nanoscale*, 2014, **6**, 908-915.

- 
- 56 G. Lui, J. -Y. Liao, A. Duan, Z. Zhang, M. Fowler, A. Yu, *J. Mater. Chem. A*, 2013, **1**, 12255-12262.
- 57 N. L. Yang, J. Zhai, D. Wang, Y.S. Chen, L. Jiang, *ACS Nano*, 2010, **4**, 887-894.
- 5 58 G. Zhu, L. K. Pan, T. Xu, Q. F. Zhao and Z. Sun, *J. Alloys Compd.*, 2011, **509**, 7814-7818.
- 59 N. L. Yang, J. Zhai, D. Wang, Y. S. Chen and L. Jiang, *ACS Nano*, 2010, **4**, 887-894.
- 60 G. Zhu, T. Xu, T. A. Lv, L. K. Pan, Q. F. Zhao and Z. Sun, *J. Electroanal. Chem.*, 2011, **650**, 248-251.
- 10